Search for new physics with same-sign isolated dilepton events with jets and missing transverse energy at CMS

M. Weinberg
Department of Physics, University of Wisconsin, Madison, WI, USA

The results of searches for Supersymmetry in events with two same-sign isolated leptons, hadronic jets, and missing transverse energy in the final state are presented. The searches use pp collisions at 7 TeV collected in 2011 by the CMS experiment.

I. INTRODUCTION

Events containing isolated same-sign dileptons are very rare in the Standard Model (SM), but can occur quite naturally in many different new physics models, including supersymmetry (SUSY) [1] and universal extra dimensions [2]. Isolated same-sign lepton pairs are thus a very clean experimental signature for new physics searches.

In addition, the analysis described in this talk requires significant missing transverse energy ($\not\!\!E_T$) and hadronic activity in the form of high-p_{T} jets. The choice of signal regions is influenced by two experimental observations. First, astrophysical evidence for dark matter [3] suggests the need for a massive, weakly-interacting stable particle which gives rise to final states with $\not\!\!E_T$. Second, new physics signals with observably large cross sections are likely to be the result of strong interactions, and we therefore expect them to be accompanied by significant hadronic activity. Aside from these requirements, our searches are as independent of the particular details of new physics models as possible.

The data used in this analysis were collected in pp collisions at a center-of-mass energy of 7 TeV by the Compact Muon Solenoid (CMS) detector at the Large Hadron Collider (LHC) in 2011. They comprise a total integrated luminosity of 0.98 fb^{-1}.

A. Same-Sign Dileptons in SUSY

An example SUSY cascade decay leading to jets, $\not\!\!E_T$, and same-sign dileptons is shown in Figure 1. The produced gluinos or squarks decay to charged gauginos, which subsequently decay to the lightest supersymmetric particle (LSP) neutralino. The mass difference between the gluinos/squarks and the charged gaugino, typically arbitrary, defines the amount of hadronic activity expected in the event. The mass difference between the gaugino and neutralino influences the lepton p_{T} spectrum. Further, there is a range of scenarios where a large production asymmetry exists between the τ lepton and the e/μ leptons. The range of mass differences motivates a variety of selection criteria in order to cover the widest possible phase space, while the possible tau production asymmetry motivates us to look specifically at events containing taus.

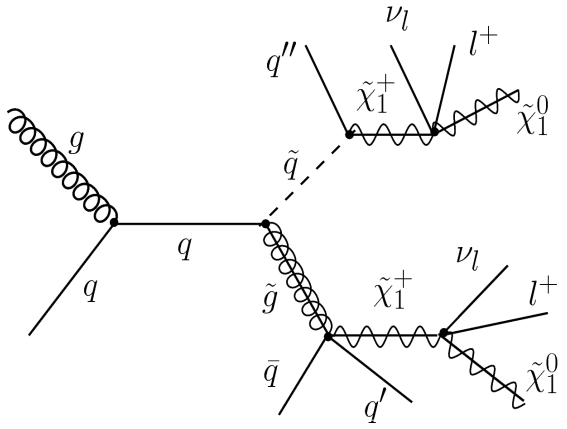

FIG. 1: An example of a process involving the production and decays of SUSY particles, which gives rise to two same-sign prompt leptons, jets, and missing transverse energy.

II. RECONSTRUCTION OF LEPTONS, MISSING ENERGY, AND JETS

Electrons, muons, and hadronically decaying taus are all included in the analysis. Lepton candidates are required to have $|\eta| < 2.4$ and to be consistent with originating from the same interaction vertex.

Electron candidates [4] consist of an energy cluster in the electromagnetic calorimeter (ECAL) matched to hits in the tracker. The identification of electrons is based on the shape of their electromagnetic shower in the ECAL as well as track-cluster matching. The criteria are designed to maximally reject electron candidates from QCD multijet production, and are approximately 80% efficient for electrons from the decay of W/Z bosons.

Muon candidates [5] must be reconstructed via two separate algorithms: Tracker muons are seeded from hits in the tracker and are matched to signals in the calorimeters and muon systems. Global muons are constructed from a simultaneous fit to hits in both the tracker and muon chambers. The identification efficiency measured in data is approximately 96% for muons of all momenta.

Jets and $\not\!\!E_T$ are reconstructed via the particle flow (PF) technique [7], which takes signals in each detector component and reconstructs physics objects from them before running jet clustering algorithms. The hadronic jets in this analysis use the anti-k_t clustering algorithm with a cone of $\Delta R = 0.5$ in $\eta - \phi$ space.

Hadronic tau candidates [6] are reconstructed starting from jets. A variable size cone of $\Delta R < 5$ GeV$/p_{\rm T}$ is defined around the leading track, and the τ decay products are required to be confined within this cone.

III. BASELINE SELECTIONS

The analysis starts from an initial selection of two same-sign leptons with $p_{\rm T} > 5, 10, 15$ GeV for muons, electrons, and taus, respectively, and $|\eta| < 2.4$. Two jets with $p_{\rm T} > 40$ GeV and $|\eta| < 2.5$ are also required, and we further require $H_{\rm T} > 80$ GeV and $\not\!\!E_T > 30$ GeV.

This initial selection is further divided into three baseline selections: The *inclusive* selection for the ee, $e\mu$ and $\mu\mu$ final states requires $H_{\rm T} > 200$ GeV. The *high-*$p_{\rm T}$ selection for the ee, $e\mu$ and $\mu\mu$ final states requires $p_{\rm T}(l_1, l_2) > 20, 10$ GeV. The tau-specific selection requires at least one of the final state particles is a tau ($e\tau$, $\mu\tau$, or $\tau\tau$) with $H_{\rm T} > 350$ GeV and $\not\!\!E_T > 80$ GeV.

A. Search Regions

We constrain the baseline selection regions with the following search regions:

- *High-*$H_{\rm T}$*, high-*$\not\!\!E_T$: $H_{\rm T} > 400$ GeV and $\not\!\!E_T > 120$ GeV, providing a high expected sensitivity to points in the Constrained Minimal Supersymmetric Standard Model (CMSSM) [8] with low values of m_0.
- *Medium-*$H_{\rm T}$*, high-*$\not\!\!E_T$: $H_{\rm T} > 200$ GeV and $\not\!\!E_T > 120$ GeV, targeting models with moderate mass-splittings between squarks/gluinos and gauginos.
- *High-*$H_{\rm T}$*, low-*$\not\!\!E_T$: $H_{\rm T} > 400$ GeV and $\not\!\!E_T > 50$ GeV, providing a high expected sensitivity to CMSSM parameter points with high values of m_0.
- *Low-*$H_{\rm T}$*, high-*$\not\!\!E_T$: $H_{\rm T} > 80$ GeV and $\not\!\!E_T > 100$ GeV, providing a high expected sensitivity to models predicting low hadronic activity with high $\not\!\!E_T$.

Figure 2 shows the events observed in data on the $H_{\rm T}$-$\not\!\!E_T$ plane for each baseline selection categories, with the dashed and dotted lines indicating the various search regions.

B. Background Estimation

Backgrounds are divided into categories based on how many prompt leptons they contain. Rare processes like $q\bar{q} \to WZ$ and ZZ, $qq \to qqW^{\pm}W^{\pm}$, $2 \times (q\bar{q} \to W)$, and $t\bar{t}W$ can produce actual prompt same-sign leptons. These are evaluated from Monte Carlo (MC) simulation and found to contribute between 10% and 40% of the total background. A 50% systematic uncertainty is applied to the value.

Processes such as $Z/\gamma^* \to l^+l^-$ and $t\bar{t}$ produce opposite-sign prompt leptons. In cases where the charge of one of the leptons is misreconstructed, these events constitute an additional background to the search. They are evaluated in data and found to contribute less than 10% to the total background.

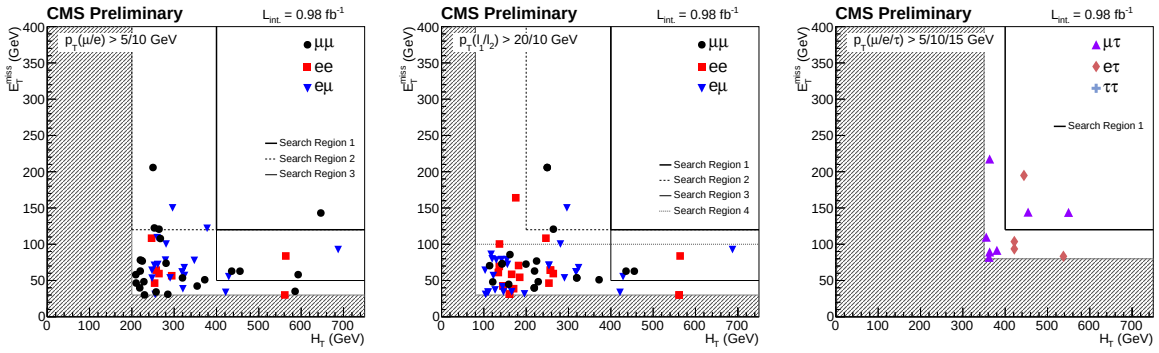

(a) (b) (c)

FIG. 2: H_{T} versus $\not\!\!E_T$ scatter plots for the three baseline regions in data: inclusive dileptons (a), high-p_{T} dileptons (b), and τ-dileptons (c).

Events with "fake" leptons from jets also contribute. Here, a fake lepton can be a lepton produced in a heavy flavor quark decay as well as a light jet that is misidentified as a lepton. This is also evaluated in data, and is found to be the dominant effect. In order to evaluate this fake rate, the analysis loosens the lepton selection criteria (such as lepton isolation requirements) to define a set of "fakeable objects". The ratio of lepton candidates passing the full selection (*tight* leptons) to lepton candidates passing this looser selection but failing the full selection (*loose* leptons) is then determined for QCD multijet events with a jet above a given threshold. This tight-to-loose (TL) ratio is shown for both electrons and muons in Figure 3.

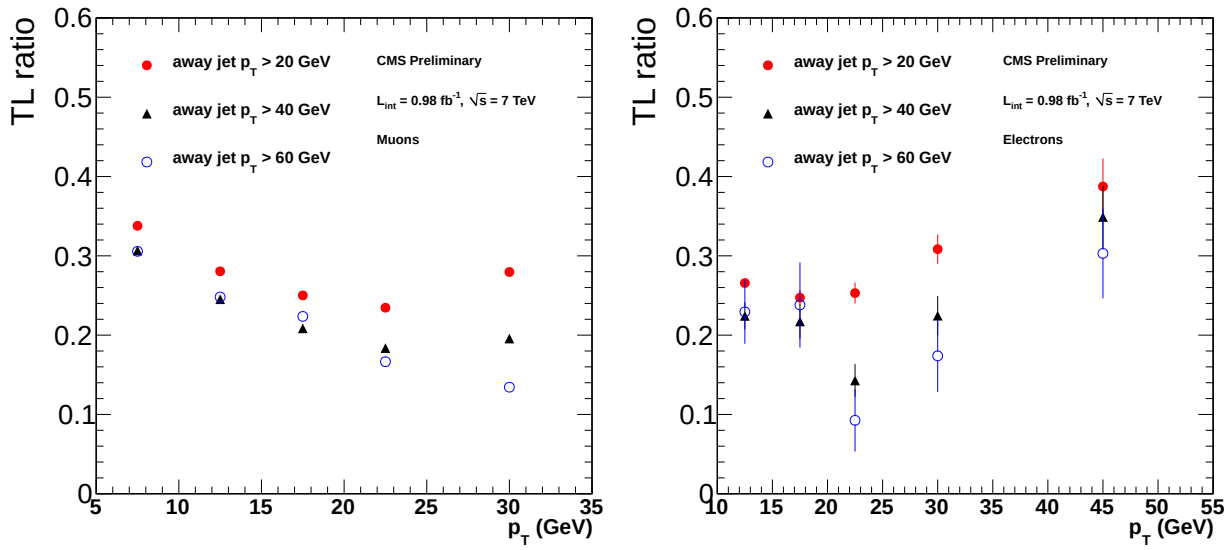

(a) (b)

FIG. 3: Muon (a) and electron (b) TL ratio projected on p_{T} using method (A1). The TL ratio distribution is displayed separately for events with a jet separated from the lepton candidate by $\Delta R > 1$ and the jet required to have p_{T} above 20, 40, and 60 GeV. The central value is measured for the case with a jet $p_{\mathrm{T}} > 40$ GeV, while the range of values measured with other jet requirements represents an estimate of the systematic uncertainty.

A summary of the background predictions as well as the number of observed events is shown for each channel in the three baseline selection regions in Figure 4. For the inclusive and high-p_{T} dilepton selections, two sets of complementary methods are used to measure the backgrounds, as indicated by the two bars associated with each

TABLE I: Observed number of events in data compared to the predicted background yields for the inclusive, high-p_{T}, and τ dilepton search regions. The uncertainties include the statistical and systematic components added in quadrature. The last row (95% CL UL yield) represents observed upper limits on event yields from new physics.

Dilepton category	**Inclusive ($H_{\mathrm{T}} > 200$ GeV)**			**High-p_{T} [$p_{\mathrm{T}}(l_1, l_2) > 20, 10$ GeV]**				**Taus**
H_{T} **(GeV)**/$\not\!\!E_T$ **(GeV)**	**400/120**	**400/50**	**200/120**	**400/120**	**400/50**	**200/120**	**80/100**	**400/120**
Predicted	2.3 ± 1.2	5.3 ± 2.4	6.6 ± 2.9	1.4 ± 0.7	4.0 ± 1.7	4.5 ± 1.9	10 ± 4	2.9 ± 1.7
Observed	1	7	6	0	5	3	7	3
95% CL UL yield	3.7	8.9	7.3	3.0	7.5	5.2	6.0	5.8

channel. These methods compare well with each other, providing mutually consistent background predictions.

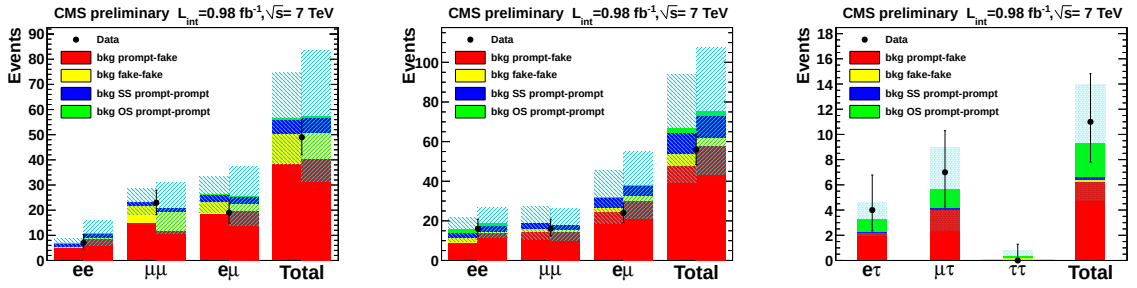

(a) (b) (c)

FIG. 4: Summary of background predictions and observed yields in the baseline region for the inclusive (a), high-p_{T} (b), and τ dilepton (c) selections. For the inclusive selections, the results of method (B) are compared with those from method (A1) in the left and right bar for each channel, respectively. For the high-p_{T} selections, the results of method (A2) are compared with those from method (A1) in the left and right bar for each channel, respectively. Predictions for events with one and two fakes (prompt-fake and fake-fake), contributions from simulated backgrounds (SS prompt-prompt), and those from events with a lepton charge misreconstruction (OS prompt-prompt) are reported separately.

IV. SEARCH RESULTS

Table I shows the events observed for each selection region, along with the total background predictions. We see no evidence of an event yield in excess of the background predictions and set 95% CL upper limits on the number of observed events using a hybrid frequentist-bayesian CL method [9] with nuisance parameters and the signal strengh maximizing the ratio of the signal-with-background to background-only likelihoods. These limits are indicated in the bottom row of the table.

V. INTERPRETATION OF RESULTS FOR NEW PHYSICS MODELS

It is necessary to convey the information shown in Table I in a form that can be used to test a variety of specific physics models. This is done by using generator-level simulation studies as approximations for the models. This was shown to be sufficiently precise to reproduce constraints on new physics models that would otherwise require the full CMS detector simulation.

We take as a benchmark point the low-mass CMSSM parameter point LM6. The efficiency of the lepton selection is shown in Figure 6 as a function of p_{T}, and the efficiency of the H_{T} and $\not\!\!E_T$ selection is shown in Figure 7 as a function of the reconstructed H_{T} and $\not\!\!E_T$, respectively. This efficiency dependence can be parametrized by error functions to determine the overall selection efficiency for new physics signals.

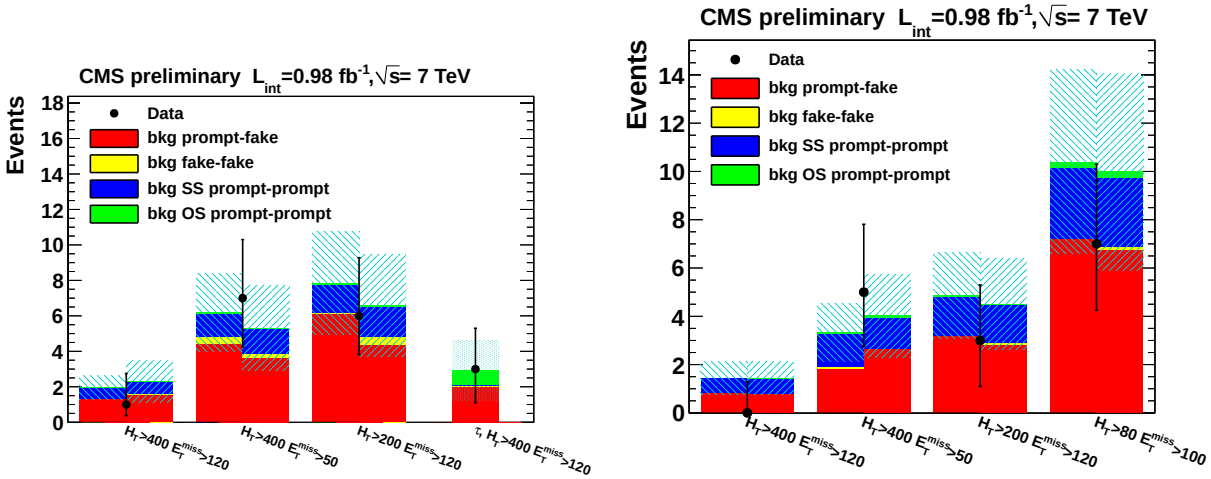

(a) (b)

FIG. 5: Summary of background predictions and observed yields in the search regions for the inclusive and τ (a) and high-p_{T} dilepton (b) selections. For the inclusive selections, the results of method (B) are compared with those from method (A1) in the left and right bar for each channel, respectively. For the high-p_{T} selections, the results of method (A2) are compared with those from method (A1) in the left and right bar for each channel, respectively. Predictions for events with one and two fakes (prompt-fake and fake-fake), contributions from simulated backgrounds (SS prompt-prompt), and those from events with a lepton charge misreconstruction (OS prompt-prompt) are reported separately.

In order to provide a reference for other SUSY searches, the results are interpreted in the context of the CMSSM model. The observed upper limits on the number of signal events shown in Table I for the high-H_{T}, high-$\not\!\!E_T$ search region of the high-p_{T} dilepton baseline selection are compared to the expected number of events in the CMSSM model in a plane of $(m_0, m_{1/2})$ for $\tan\beta = 10$, $A_0 = 0$, and $\mu > 0$. All points on this plane with mean expected values in excess of this limit are interpreted as excluded at the 95% CL. This excluded region is shown in Figure 8. The shaded region represents the uncertainty on the position of the limit due to uncertainty in the production cross section of CMSSM.

VI. SUMMARY AND CONCLUSIONS

A search for new physics was performed in the same-sign dilepton channel, including final states with electrons, muons, and taus. All major background sources were estimated directly from data. Events with a single fake lepton were found to be the dominant background in all channels of the search with the exception of the $\tau\tau$ channel, where two fake τ leptons were the primary background contribution.

No evidence was seen for an excess over the background prediction. We therefore set 95% CL upper limits on the number of signal events within $|\eta| < 2.4$ with 0.98 fb^{-1} of data. These limits are reported as an exclusion curve in CMSSM parameter space.

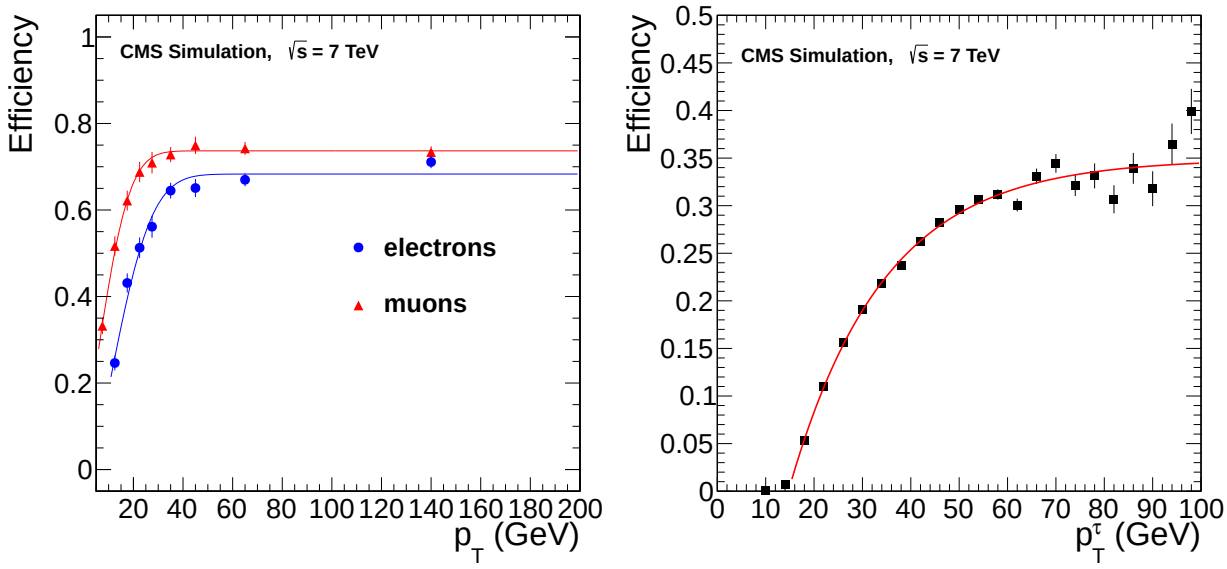

(a) (b)

FIG. 6: Electron (a) and muon (b) selection efficiency as a function of p_{T}, estimated in simulation LM6 benchmark point and corrected for simulation-to-data scale factors.

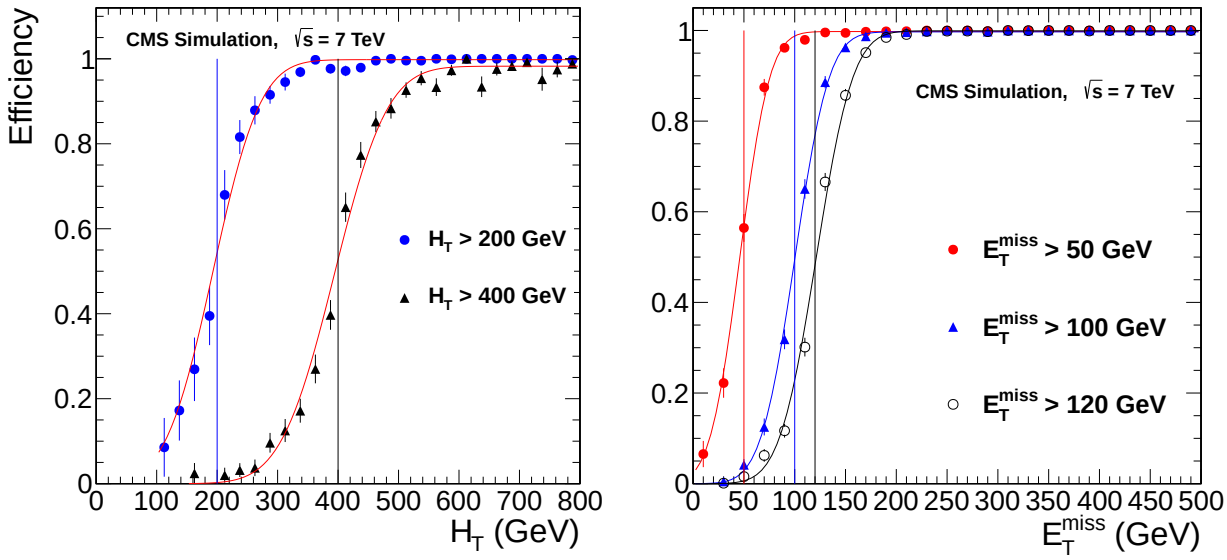

(a) (b)

FIG. 7: Efficiency for an event to pass a given reconstructed H_{T} (a) and $\not\!\!E_T$ (b) threshold as a function of generator level H_{T} and $\not\!\!E_T$. The curves are shown for $\not\!\!E_T$ thresholds of 50, 100, and 120 GeV; the thresholds for H_{T} are 200 and 400 GeV.

[1] R. Barnett, J. Gunion, and H. Haber, "Discovering supersymmetry with like sign dileptons", *Phys. Lett.* **B 315** (1993) 349.
[2] H. Cheng, K. Matchev, and M. Schmaltz, "Bosonic supersymmetry? Getting fooled at the CERN LHC", *Phys. Rev.* **D 66** (2002) 056006.

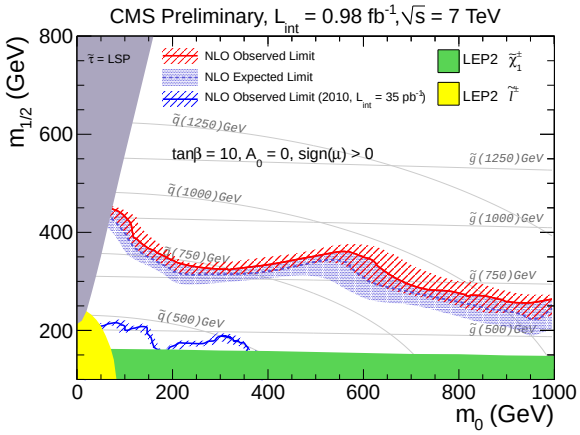

FIG. 8: Exclusion region in the CMSSM corresponding to the observed upper limit of 3.0 events in the search region 1 of the high-p_{T} dilepton selections. The result of the previous analysis is shown to illustrate the improvement since 2010.

[3] G. Bertone, D. Hooper, and J. Silk, "Particle dark matter: Evidence, candidates and constraints", *Phys. Rept.* **405** (2005) 279.

[4] CMS Collaboration, "Electron reconstruction and identification at $\sqrt{s} = 7$ TeV", *CMS Physics Analysis Summary* **CMS-PAS-EGM-10-004** (2010).

[5] CMS Collaboration, "Performance of muon identification in pp collisions at $\sqrt{s} = 7$ TeV", *CMS Physics Analysis Summary* **CMS-PAS-MUO-10-002** (2010).

[6] CMS Collaboration, "Performance of tau reconstruction algorithms in 2010 data collected with CMS", *CMS Physics Analysis Summary* **CMS-PAS-TAU-11-001** (2011).

[7] CMS Collaboration, "Particle-Flow Event Reconstruction in CMS and Performance for Jets, Taus, and $\not\!\!E_T$", *CMS Physics Analysis Summary* **CMS-PAS-PFT-09-001** (2009).

[8] G. Kane et al., "Study of constrained minimal supersymmetry", *Phys. Rev.* **D 49** (1994), no. 11, 6173.

[9] Particle Data Group Collaboration, "Review of particle physics", *J. Phys.* **G 37** (2010), 075021.